Available online at www.sciencedirect.com

jmr&t Journal of Materials Research and Technology

journal homepage: www.elsevier.com/locate/jmrt

Original Article

Study of mechanical, durability and microstructural properties of cementitious composite with addition of different iron ore tailings from Brazil

Bruna Silva Almada [a], *Henrique da Silva Silveira Melo* [b], *Marlo Souza Duarte* [b], *Maria Teresa Paulino Aguilar* [b], *Dayana Cristina Silva Garcia* [b], *Guilherme Jorge Brigolini Silva* [a], *White José dos Santos* [b,*]

[a] *Laboratory of Materials for Civil Construction, Federal University of Ouro Preto, Ouro Preto, Minas Gerais, Brazil*
[b] *Department of Materials Engineering and Construction, Federal University of Minas Gerais, Belo Horizonte, Brazil*

ARTICLE INFO

Article history:
Received 22 January 2022
Accepted 9 March 2022
Available online 23 March 2022

Keywords:
Iron ore tailings
Waste heterogeneity
Mineral addition
Waste reuse
Mechanical properties
Durability

ABSTRACT

Brazil is the second-largest global iron ore producer in the world. Consequently, a large volume of iron ore tailings (IOTs) is generated, which is associated with environmental impacts. IOTs present potential to be used as an addition in cementitious compounds, however, few studies assess how the heterogeneity of this waste can limit its utilization as a building material. Thus, the present study aims to assess whether the heterogeneity of IOTs influences mechanical, durability, and microstructural properties when added to the cementitious composite. Four IOTs samples from different origins were collected and added to cementitious composite at 40% addition content. Composites' mechanical (compressive strength and modulus of elasticity) and durability properties (water absorption, porosity, electrical resistivity, carbonation, and pH pore solution) were correlated to the microstructure of the IOTs. Results showed that the IOTs from different mines exhibited different physical properties and chemical/mineralogical compositions. Moreover, the higher the degree of ore processing, the lower the heterogeneity, iron content, and specific gravity. Although the IOT samples are heterogeneous, this type of tailing can be used as a filler addition in structural mortars. IOT addition tends to improve the mechanical and durability properties. Heterogeneity most significantly influenced the properties in the fresh state, durability, and microstructural properties. The microstructure of the cement matrix tends to be denser in the IOT-added with higher SSA and silica content. Was observed higher-porosity in regions close to the interfacial transition zone in the samples with coarser IOT.

* Corresponding author.
E-mail address: white.santos@demc.ufmg.br (W.J. dos Santos).

https://doi.org/10.1016/j.jmrt.2022.03.070

1. Introduction

According to the United States Geological Survey [1], Brazil holds almost 19% of all iron ore deposits in the world (average iron content higher than 55%). As a result, Brazil is the second-largest producer of that mineral while Australia holds the first position in this ranking. Brazil produces 430 million tons of processed ore, contributing approximately 16% of the national industrial GDP [2]. However, iron mining is also associated with environmental impacts [3–5]. It is estimated that every ton of processed iron ore generates 0.4 tons of tailing. In some cases, the amount of tailing may be much greater [6,7]. Consequently, the large amount of waste generated (often deposited in dams), is associated with major environmental disasters [3–5]. As example, in 2015, there were two dam failures in the city of Mariana, State of Minas Gerais, Brazil. Consequently, 62 million cubic meters of tailing were released, which reached areas up to 100 km from the accident location [3]. Shortly after, in 2019, another dam broke in the city of Brumadinho, state of Minas Gerais, Brazil, and released 12 million cubic meters of tailing killing 240 people [4]. Within this context, IOT reuse is a way to improve the production process in mining companies by reducing residue production and its environmental impacts [5–7].

The civil construction sector needs to produce more efficient and high-performance materials, which can contribute to environmental sustainability [8–12]. Thus, the use of an industrial by-product, such IOT, as a mineral addition has great relevance. The IOTs present potential to be used as building material due to their granulometry and chemical composition [13]. According to Peixoto et al. [14], IOTs are technically, economically, and environmentally feasible to produce various products, such as: ceramic materials [14,15], materials for road constructions [16], geopolymer mortars [17], ink for paint [18] and ecological brick [15] and cementitious composites [19–42].

In literature, the IOT is often used as an aggregate in cementitious composites [19–30] due to its high quartz content, inert material, and particle size closes to sand [5,8]. Natural aggregate replacement by aggregate wastes decreases the natural sand extraction. Furthermore, the IOT can also be used as a mineral addition or cement replacement. However, in this case, it is required a granulometry adjustment (particles <0.075 mm) [31–39] or any thermal activation [31,35–37].

In general, when 20% of natural aggregate is replaced by IOT aggregate an increase is observed in mechanical properties of cementitious compound. However, these properties tend to decrease when replacement values reach above 40% [19–30]. On the other hand, when the IOT is used as a binder replacement, the mechanical properties tend to decrease with increasing IOT content, since the amount of reactive material (cement Portland) decrease [31–39]. Therefore, replacement values tend to be low (<10%). Furthermore, the most satisfactory results were obtained when mechanic-thermal treatments were performed [34]. However, the implementation of these treatments requires a great amount of energy and heat [5], increasing the costs and reducing the sustainable character of the research. Regarding using IOT as an addition (without cement replacement), without activation process and just with comminution in a mill, there are few studies. The available literature points to an application in higher contents (up to 40%), with maintenance of mechanical properties [40–42]. Thereby, the exploration of the mechanical properties and durability indicators of cementitious composites with high additions of IOT will contribute to know the effects of the residue in this application.

In general, IOTs are fine, dense and crystalline materials, whose main constituents are iron, silicon and aluminum [40,41]. However, these tailings can present great variability on their physical and chemical properties, due to deposits' geological nature differences and to different ore processing methods [12,42]. For example, iron contents close to 10% are found in IOTs coming from Chinese ore [19–22,26–35,37–39,42], however, Brazilian IOTs have much higher iron contents [5,8–18,23–25,36,40,41]. Although China is an important country for iron ore production in the world, its deposits have low iron concentration [1], which justifies the low content of iron in its ore tailing and process with more complex and more expensive processing. Additionally, many researches [19–41] study one or two types of IOTs and do not present or consider the effects of the characteristics of mining and processing [19–41].

Thus, it is essential to develop new studies on Brazilian IOT's influence on properties of cementitious products. For this reason, it is important to examine the influence of IOT additions (in natura or with slight comminution) on durability and microstructure of cementitious composites. Therefore, the aim of the present study was to determine chemical, physical, mineralogical and microstructural characteristics of Brazilian IOTs and evaluate whether the heterogeneity of these (added) wastes influences the cementitious composite (structural mortars). Four IOT samples, from different origins and processing process, were collected and characterized. The mechanical resistance, water absorption and porosity, modulus of elasticity, electric resistivity and resistance to carbonation of structural mortar with IOT-addition were evaluated. These properties were correlated to the chemical, physical, mineralogical and microstructural characteristics of IOTs.

2. Materials and experimental program

2.1. Materials

Cement Portland CPI (Ordinary Portland Cement), standard quartz sand, and four IOT were used in this research. Four iron ore tailing from different mines and generated on different processing were used in the experiment, as shown in Table 1. It is worth highlighting that all IOT samples were ground in a PAVITEST (Contenco Indústria e Comércio LTDA) mill, with 42 steel bars, for 15 min.

2.2. Powder characterization

The aim of the present study was to characterize the waste as completely as possible. For this reason, their chemical,

Table 1 – Description of IOT samples.

Sample	IOT origin/processing	Collection point
SF	Processing for sinter feed production	Pile
BS	Processing only based on crushing, screening, and dewatering cycles	Dam
BC	Processing based on flotation and magnetic separation steps	Dam
AR	Processing based on two flotation stages (high quartz content)	Tailings thickener

physical, mineralogical and microstructural composition was assessed, according to Table 2.

2.3. Structural mortars mix

Structural mortars were molded to verify the effects of the IOT characteristics on their properties in the fresh and hardened state. For this, proportion of materials (1:0.40:3—cement: IOT: sand) and water-to-cement ratio (0.5) were fixed. It is worth noting that the tailings were added at 40% of content (in relation to the cement mass), without replacing the cement. Thus, the variables of each specimen were just the properties of each IOT sample. The IOT content was defined according to previous research [41] which showed that, after varying several IOT contents, 40% was a promising value, concerning to mechanical and durability properties.

The samples were prepared according to NBR 7215 Standard [43]. The freshly mixed cementitious composite was placed in steel molds and vibrated using a vibrating table. The densification by vibration stopped when uniform bleeding was observed in each layer. The three-layer densification was applied to cylindrical specimens (Ø5 × 10 cm), five-layer densification was adopted for specimens (Ø5 × 10 cm) and the two-layer one was applied to prismatic specimens (4 × 4 × 16 cm). After casting, all samples were stored in a curing room (>90% RH) for 48 h ± 10 h before demolding. Then, the samples were identified and cured in humid chamber, for 28 days.

2.4. Structural mortars characterization

The Flow table test was used to determine consistency of fresh cementitious composite, according to BS EN 1015-3 Standard [44]. In the hardened state, mechanical properties, some durability parameters and microstructure were analyzed, according to methods described below.

Compressive strength was determined at 28 days, in a Contenco press, at a load rate of 0.5 MPa/s and pressure of 0.1 kgf, as recommended in BS EN 1015-11 Standard [45]. The dynamic modulus of elasticity was determined in dry specimens at 28 days, according to forced resonant frequency method in longitudinal mode, on recommendations in the C215 Standard [46] and on considerations by Lee et al. [47]. Erudite MKII Resonant Frequency Test System equipment, adjusted to frequencies ranging from 7000 to 14,000 Hz and to tension of 0.50 V, was used in this test.

The volumetric electrical resistivity was measured in saturated specimens through potential difference on flat surfaces, after 28 days according to NBR 9204 [48]. Digital function generator FG-8102 (Politerm), with 8V was used. Carbonation study was carried out through the phenolphthalein indicator solution (1%) method, according to CPC-18 [49] and ISO 1920-12 [50] recommendations. Carbonation chamber with 5% CO_2, 27 °C ± 2 °C, and humidity of 65% ± 5% was used, where specimens remained in for 85 days.

Pore solution pH in carbonated cementitious composite was assessed through the suspended powder method [51]. Powder was extracted from the specimens after longitudinal disruption, with the aid of a drilling machine and a brush. Powder extraction was carried out in the internal intermediary region (IIR), located 1 cm from the edge, in internal central region (ICR), located 2 cm from the edge, and in an external region (ER) close to the edge. Holes were approximately 3 mm in depth. Deionized water, at water-soil ratio of 20:1, was used for suspension. Samples pH was measured in BioVera PB18000 pHmeter, after 24 h agitation.

Water absorption was determined through immersion and by capillarity of samples after 28 days of cure. Procedures were described in standards ASTM C642-13 [52] and BS EN 1015-18 [53]. The total porosity was calculated from Eq. (1), based on Archimedes' principle. Theoretical density of the cementitious composite can be calculated through the mean specific mass of materials (Eqs. (2) and (3)).

$$P_t = [1 - ((p_w \times M_{dry})/(\rho_{theoretical} \times (M_{sss} - M_i))] \times 100 \quad (1)$$

$$P_{theoretical} = f_c \times \gamma_c + f_a \times \gamma_a + f_b \times \gamma_b \quad (2)$$

$$f_i = i/(1 + a + b) \quad (3)$$

Wherein:

P_t = total porosity (%)
ρ_w = water density (g/cm^3)
M_{dry} = specimen dry mass (g)
Msss = dry-surface saturated specimen's mass (g)
Mi = specimen's mass immersed in water (g)
$\rho_{theoretical}$ = Theoretical density (g/cm^3)
fi = mass fraction of the material, with i = 1 for cement, i = a for aggregate, i = b for addition
a = fine aggregate ratio in relation to cement mass
b = Mineral addition ratio in relation to cement mass
γ_c = cement specific mass (g/cm^3)
γ_a = fine aggregate specific mass (g/cm^3)
γ_b = mineral addition specific mass (g/cm^3)

In addition, a cross-sectional cut was made at half of cylindrical specimens' samples to visualize the spatial distribution, dimension and pore shape in the samples. Pores in the cementitious composite were highlighted with black pen and photographed in digital microscope (1600× magnification).

For microstructural evaluation, SEM-BSE images were analyzed in a Quanta 3D FEG-SEM. The hydrated products and

Table 2 – Description of materials characterization methods used.

Characterization	Technique/method	Equipment	Conditions
Chemical composition	X-ray fluorescence	Magic Fast Panalytical	Lithium tetraborate fusion, and loss to ignition (LOI) by sample calcination at 1000 °C
Mineralogical composition	X-ray diffraction	Philips PW 1710	CuKα (λ = 1.54 Å, V = 50 kV, 30 mA), and step size of 0.02°/s. Software HighScore Plus and Crystallography Open Database (COD) minerals database were used for phase identification.
Particle size distribution	Laser granulometry	Bettersize 2000 granulometer	Dispersant: water
Microstructure	Scanning electron microscopy	SEM-VEGA3 -Tescan equipment	Metallization: Gold 20 kV Backscattered Electron
Specific Gravity	Pycnometer method	Quantachrome SPY-3 pycnometer	Helium gas
Specific surface area and material porosity	BET and DFT methods were used for SSA and porosity, respectively	Quantachrome NovaWin-Data Acquisition and Reduction (Nova Instruments)	N2 (g) adsorption method with pressure tolerance of 0.050/0.050 (adsorption/desorption)

IOT particle identification in composites matrix was assessed through the contrast of SEM-BSE images and by chemical mapping in EDS INCA X-act detector (Oxford – Instruments). It is known that flat polished section minimizes topographic contrast since high spots appear bright in SEM-BSE images [54,55]. For this reason, samples extracted from specimens' internal region were embedded in acrylic resin and polished with silicon carbide papers (#800, #1200, #1500 and #2000) and diamond pastes (9 μm, 3 μm and 1 μm), with Isopropyl Alcohol as a lubricant. The samples were cleaned in alcohol under ultrasonic vibration between grinding and polishing steps. SEM-BSE images were processed using ImageJ software to obtain the porosity, and pore size distribution, based on Ferret diameter. Cracks were erased to avoid mistaking considerations on Ferret diameter. It is important to highlight only pores equal to, or bigger than, 1 pixel could be identified [56].

3. Results and analyses

3.1. *Chemical and mineralogical composition*

The CEM I and IOTs chemical composition are shown in Table 3. It is observed that IOTs are composed mainly by Fe_2O_3 and SiO_2. In these samples, iron content ranged from 44.80% (AR) to 81.21% (SF) and silica content ranged from 10.60% (SF) to 54.10% (AR). SF and BS tailings presented slightly higher alumina content (Al_2O_3) than the other ones, suggesting the presence of clay minerals in their composition. Moreover, the loss of ignition (LOI) in these samples (SF and BS) was also higher. It is known that dehydroxylation of goethite (FeOOH) takes place between 200 °C and 3000 °C and forms hematite (Fe_2O_3) [40]. Thus, this mineral is expected to be more abundant in SF and BS. Overall, higher iron contents were found in samples whose ores of origin were less processed (SF and BS), whereas the highest silica contents were identified in samples presenting higher ore processing (BC and AR). This result points to a heterogeneity between the samples and shows the dependence of the chemical composition of the material on ore processing, as well as on its collection location.

The mineralogical composition of IOT samples was assessed through XRD (Fig. 1). The results show that all samples had high crystallinity. This is indicative of low reactivity degree, or no reactivity at all, similarly to results of the literature [9,33,40,41]. Furthermore, studies have pointed out that IOT has a low pozzolanicity degree, even when it is chemically or mechanically activated [40,41].

The mineral phases present in samples were quartz (SiO_2), hematite (Fe_2O_3), goethite (FeO), gibbsite (Al_2O_3), kaolinite ($Si_2Al_2O_5(OH)_4$) and magnetite ($FeO.Fe_2O_3$), which are in accordance with the XRF chemical analysis. These minerals were the ones typically found in Brazilian iron ore and tailing [9,33,40,41]. Studies carried out with IOT from different origins identified other minerals, such as chlorite ($(Mg, Fe)_3(Si, Al)_4O_{10}(OH)_2 \cdot (Mg, Fe)_3(OH)_6$), hornblende ($(Ca, Na)_{2-3}(Mg, Fe, Al)_5(Al, Si)_8O_{22}(OH, F)_2$), diopside ($Ca(Mg, Fe)Si_2O_6$), meixnerite ($Mg_6A_{l2}(OH)_{16}(OH)_{2.4}H_2O$)—which are found in Chinese IOT [27,57] —and chamosite ($(Fe^{2+},Mg,Fe^{3+})_5Al(Si_3Al)O_{10}(OH,O)_8$) —which is found in Malaysian IOT [25], although they were not at major phase. This finding highlights that IOT

Table 3 – Chemical composition (wt. %) of the materials.

	Fe_2O_3	SiO_2	Al_2O_3	CaO	MgO	TiO_2	P_2O_5	Na_2O	K_2O	MnO	BaO	LOI
SF	81.21	10.60	3.04	0.06	<0.1	0.08	0.18	<0.1	0.02	0.32	<0.01	4.94
BS	74.20	18.30	1.83	0.03	<0.1	0.08	0.16	<0.1	0.03	0.31	<0.01	4.22
BC	49.61	49.80	0.51	0.03	<0.1	0.08	0.013	<0.1	0.01	0.12	<0.01	0.62
AR	44.80	54.10	0.43	0.06	<0.1	<0.01	<0.005	0.43	0.05	<0.008	<0.01	0.11
CEM I	2.38	19.90	4.34	63.30	2.68	0.23	0.23	0.17	0.98	0.05	–	2.29

heterogeneity is related to different characteristics of deposits where raw ores are collected.

Major phases are different in each IOT, as evidenced by the semi-quantitative results recorded for the mineralogical composition, shown in the right side of Fig. 1. From the results, it possible to infer that the higher the degree of ore processing, the more representative the quartz content and the lesser representative the hematite content. Moreover, it can be observed the important role played by the magnetic roller used to process ore, which has generated SF tailing at magnetite separation. Magnetite was not identified in the composition of this sample, despite its small processing. Thus, processing influences tailing heterogeneity.

Figure 2 (SEM-EDS) clearly show iron content reduction in particles of tailing coming from ore subjected to several processing stages (BC and AR). This finding confirms the XRF results. Sample SF (Fig. 2) presented a large amount of small and lamellar particles adhered to the surface of bigger grains. These small particles were composed either of iron, or of silicon and aluminum. Therefore, they were associated with iron oxides, such as hematite and goethite, and clay minerals, such as kaolinite ($Al_2O_{3.2}SiO_{2.2}H_2O$) and gibbsite ($Al(OH)_3$), identified through XRD. The bigger particles, which were mainly formed by silicon, were associated with quartz. These characteristics were identified in BS tailing. For the samples BC and AR, mostly silicon-rich and bigger particles (quartz) were observed.

From Fig. 2, it can be said that all samples showed the same (irregular shape) particle morphology, as already presented in the literature [9,33,40,41]. However, other physical aspects depend on the mineralogical composition and on the beneficiation, process applied to the raw ore, such as granulometry, specific surface area and porosity. These physical properties will be described below.

3.2. *Physical properties of IOT*

Particle size distribution of IOT (Fig. 3) presented a high number of particles bigger than cement, even after being ground and, in general, the IOTs studied were rougher than IOT samples used as addition or as binder replacement assessed by other authors [33,40,41]. It was possible to observe similarity between samples SF and BC, and samples BS and AR, despite the mineralogical difference. It is noteworthy that the SF and BC tailings presented closer granulometric to that of the CEM I cement, mainly in fractions smaller than 5 μm, as well as more varying discrete distribution of particles. On the other hand, the BS and AR tailings presented lesser heterogeneous granulometry and particle concentration ranging from 40 μm to 150 μm. Moreover, the AR sample presented the greatest amount of quartz (high hardness mineral), which explain the greater particle granulometry after milling. In addition, this sample was generated after several processing steps and, due to the collection location (tailing thickener after flotation), the lowest granulometric variety can be justified by tailing separation during previous processing stages. Therefore, it is possible to notice that granulometric variation in IOT

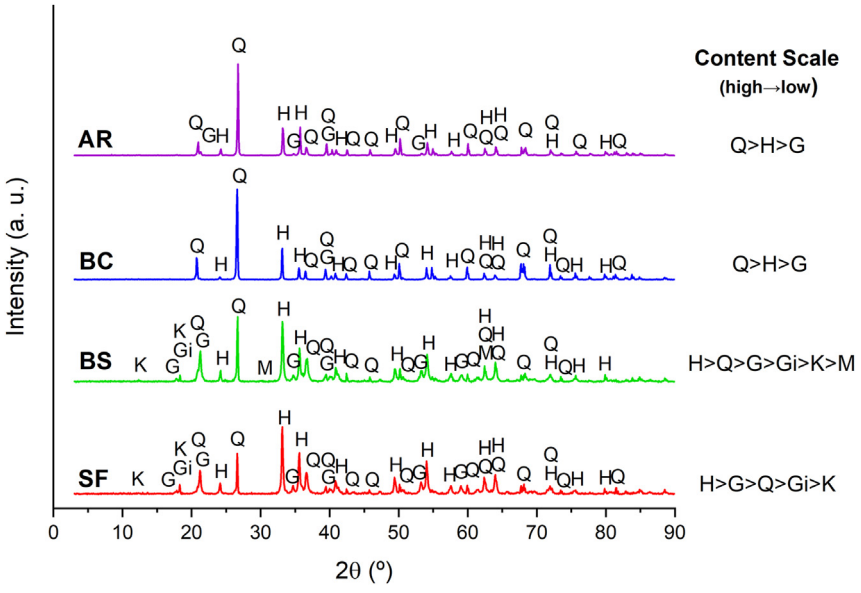

Fig. 1 – Diffractograms of iron ore tailings samples. (Q – Quartz; H – Hematite; G – Goethite; Gi – Gibbsite; K – Kaolinite; M – Magnetite).

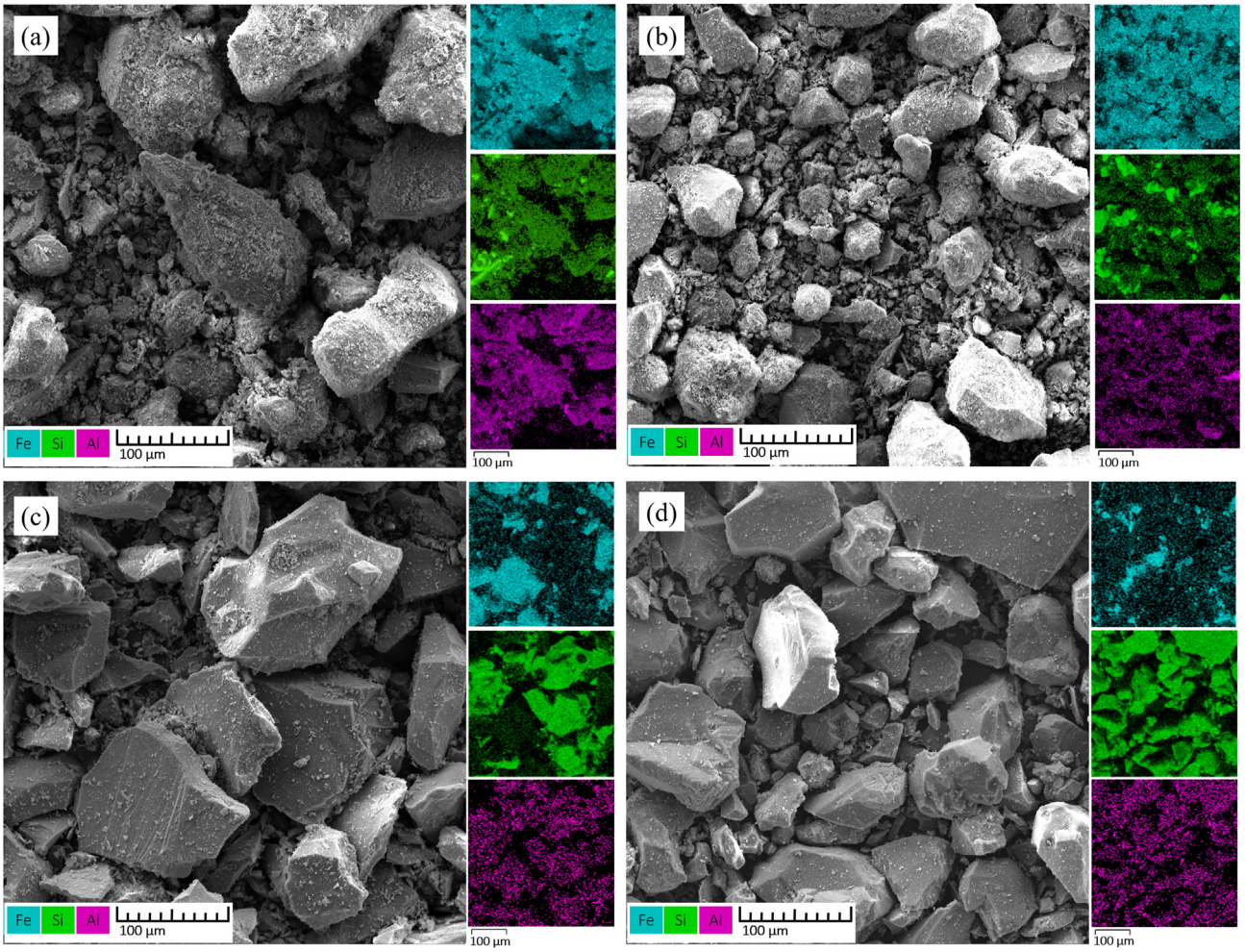

Fig. 2 – Chemical mapping (SEM-EDS) of the IOT sample (a) SF, (b) BS, (c) BC and (d) AR.

particles is indicative of the geology inherent to different regions, as well as of different material preparations.

Table 4 presents the specific mass, specific surface area (SSA) and porosity of cement and IOT. Specific mass values were high in tailings from processing based on less stages (SF and BS): 4.234 g/cm^3 and 4.359 g/cm^3, respectively, which can be 35% higher than that of cement (3.221 g/cm^3). This result can be explained by the higher iron content in these samples, as shown by the XRF analysis. On the other hand, tailing AR (highly processed ore) recorded specific mass lower than that of cement, due to reduced content of this element in its composition. Results found in the current study are within values presented in the Brazilian literature [8,9,41]. However, in comparison to IOT from Chinese ore, and from other countries [30,35], specific masses were slightly higher, mainly in tailings SF and BS.

Given the presence of a large number of fine particles adhered to the bigger particles, which increases material porosity, samples SF and BS presented the highest SSA: 8.750 and 10.107 m^2/g, respectively. These values were 5–8 times higher than results recorded for other IOT samples. On the other hand, samples BC an AR recorded SSA values close to those of cement: 1.199 and 1.730 m^2/g, respectively. These values can be justified by the high concentration of quartz, whose particles are smooth and present coarser particle size. Likewise, the total volume of pores and mean radius of SF and BS samples were higher.

Despite the AR sample not being the one recording the smallest specific surface, it was identified as the least porous and with the smallest pore radius. This finding can be attributed to AR's lower mineralogical and granulometric heterogeneity. Yunhog et al. [33] highlighted that longer grounding times lead to particle agglomeration due to increased surface energy, which reduces the specific area of the material.

3.3. *Consistency index*

Fig. 4 presents the consistency index of all structural mortars. It is observed that the addition of 40% of IOT in mortars and the same w/c ratio decreased workability in all cementitious composites. Despite the reduced consistency (22.5%, at most), it was decided not to use a plasticizer admixture in this present study, since it was possible to prepare the samples. As highlighted by Fontes et al. [9] and Castro [41], the higher the IOT ratio, the higher the amount of required water, and this effect is more evident when the composites present more than 20% of IOT addition. Furthermore, irregular-shaped and greatly porous IOT particles account for the high demand for water [28]. Therefore, this result was expected.

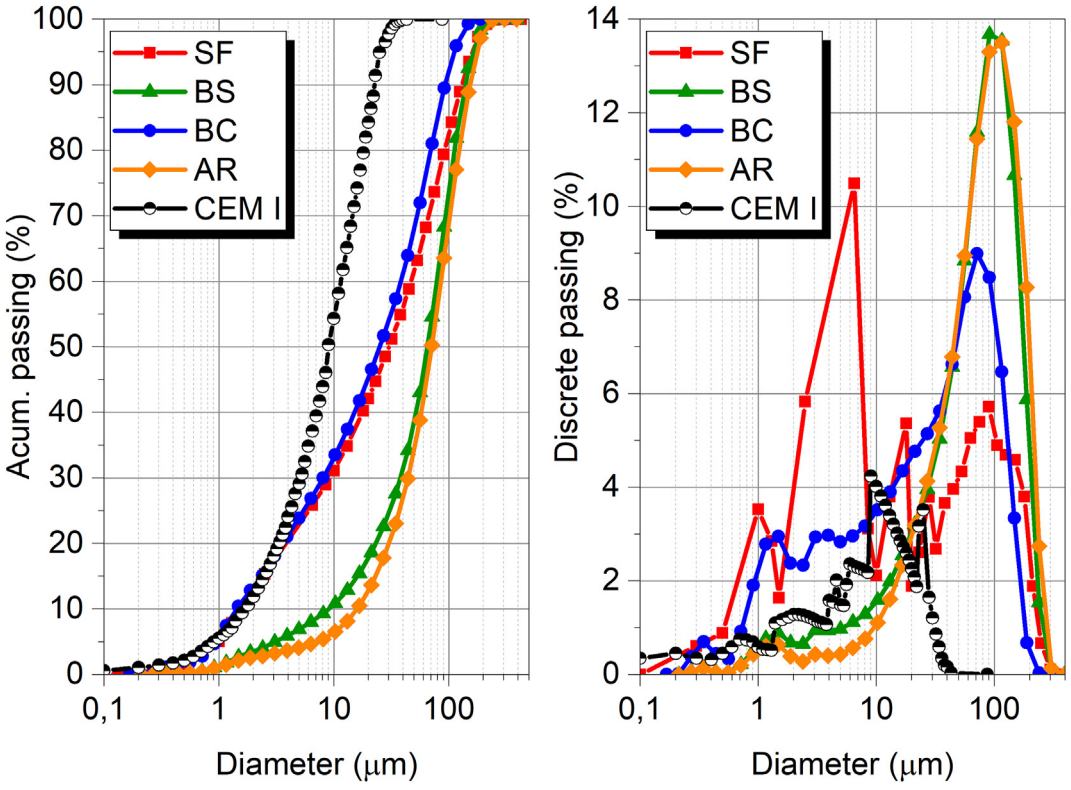

Fig. 3 – Accumulated and discrete particle size distribution of IOTs particles.

The water demand of the IOTs was slightly higher than that of cement, but it was possible noticing that each IOT sample affected the composite consistency at a different level. Thus, the IOT heterogeneity had influence in this property. As consequence of the differences in the fineness and specific mass of IOT samples, the solid volume in composites was variable, which affected the water demand. Table 5 shows the variation in the solid volume, water volume and on the area of fines in each sample. Materials' consumption, specific mass and specific surface area were taken into account to reach parameters. Cement and IOT were taken as the solid fines in the composition.

Cementitious composite BS40 presented drier consistency, almost no spreading on the table and small cohesion loss, although it remained plastic. Despite the high addition content and the high specific mass of BS tailing, its use only increased the volume of solids in the mortar by 23.71%. Nevertheless, its specific surface and quite high porosity have contributed to significant increase in the area of fines, or "wetting area" (221.91%). This process resulted in increased demand for water and in greater workability reduction in cementitious composite (22.55%). The same happened in the SF40 composite, however, the differences in particle size distribution between BS and SF tailings may have contributed to keep the consistency of SF40 a little closer to that of the reference cementitious composite. Oppositely, tailings BC and AR, which recorded a lower specific mass and specific surface area, had a greater impact on increasing the volume of solids and less effect in the "wetting area". Differences in granulometry and porosity also contributed to the proximity of the results between SF40 and BC40.

3.4. *Water absorption and porosity*

Fig. 5 shows the water absorption, porosity and capillarity coefficient of structural mortars. In all samples, water absorption was lower than 10%, indicating a good composite durability [60]. The introduction of IOTs in the cementitious composite led to a slight reduction in water absorption (max. 14.6% in AR40) and porosity (max. 6.6% in BC40). Overall, the use of IOTs resulted in the maintenance and in small improvements in the durability of cementitious composites. This

Table 4 – Specific surface area and material porosity.

Sample	Specific mass (g/cm^3)	SSA (m^2/g)	Total volume of pores (10^{-3} cm^3/g)	Mean radius of pores (Å)
SF	4.234	8.750	12.540	50.310
BS	4.359	10.107	16.850	69.035
BC	3.489	1.199	1.625	43.216
AR	2.807	1.730	1.331	21.829
CEM I Cement	3.221	1.705	2.899	74.234

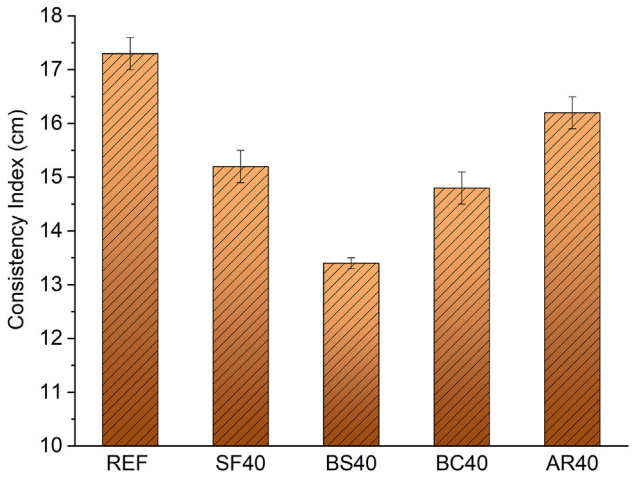

Fig. 4 – Consistency index of cementitious composite.

result is associated with the fineness of the IOTs, which occupies either macro or micro pores [25]. Equivalent results were observed by Castro [41], whose study has shown the trend of reducing the emptiness index and water absorption due to increase in IOT addition content, since it acts as a filler.

There was not a significant variation in water absorption in the IOT-added samples, and it evidences that heterogeneity of the IOTs does not have strong impact on this property. Based on the results, some physical properties of IOTs, such as porosity—which presented significant difference between samples, seem not to be important for the absorption and porosity of the cementitious composite. However, it is noteworthy that open porosity and capillarity coefficient presented an important variation among samples, mainly in BC40 and AR40. The results indicated that SF40 and BS40 samples presented a coefficient very close to the reference sample, only with an increase of 6.09% and 5.81%, respectively. However, BC40 and AR40 samples reached much higher increases (45.58% and 109.03%, respectively).

Although sample BS40 recorded higher consistency loss, which implies in higher densification and increase of microporosity, both high porosity and IOT specific surface area have reduced exudation in the mix. Thus, connectivity of smaller pores decreased, and capillary absorption remained close to that of the reference cementitious composite. The opposite was observed in sample AR40, which, despite the lower workability loss, presented exudation and higher capillary absorption. Therefore, it is inferring that, in this case, the physical properties of IOTs have influenced (increased) capillarity in the cementitious composite.

3.5. *Macro and microporosity by image analysis*

Based on these results, it can be said there is a difference in the size, shape and/or spatial distribution of pores in hardened cementitious composites. Regarding these aspects, it is possible to highlight the effect of two main factors: the filler effect of the IOTs (filling the smallest pores) and the influence of the IOT on cementitious composite workability, which affects layer densification (amount and distribution of the biggest pores). According to Mehta and Monteiro [58] pores bigger than 3 mm derive from air imprisonment during the mixing process. To evaluate these effects, images of cross-sectional sections of specimens Ø5 × 10 cm (digital microscope) and of polished samples (SEM-BSE), with emphasis on pores observed in the ImageJ software were analyzed (Fig. 6).

From digital microscope images, it was observed that the reference cementitious composite (Fig. 6a) had pores with circular sections and presented uniform spatial distribution, while IOT-added samples (Fig. 6c, e, g and i) showed pores slightly more irregular, with lower spatial-distribution uniformity. This effect can be attributed by consistency reduction in the cementitious composite. SEM-BSE images (Fig. 6b, d, f, h and j) showed that the reference cementitious composite presented bigger pores, whereas the cementitious matrices of IOT-added samples were denser and had more porous locations. There was pore refinement and filling due to IOT addition. It was also possible noticing extensive and ramified cracks in all samples.

Pore diameter distribution at two scales is presented in Fig. 7. Images of specimens' sections (Fig. 7a) indicated similar behavior among all samples. However, IOT-added samples presented bigger pores than the reference sample, mainly the samples BC40 and AR40. Although sample BS40 recorded the lowest consistency index, it presented great concentration of smaller pores. This finding is indicative of both particles packing and better mechanical resistance. Fig. 7b presents the pore diameter distribution results for SEM-BSE images. It is worth noting that the pore size evaluated corresponds to the capillary porosity range. The highest concentration of smaller pores in cementitious composite AR40 and BC40 justified the higher capillarity coefficient observed in the water absorption test.

Comparing the methods used to measure porosity in this study, image analysis showed numerically smaller results.

Table 5 – Volume and area of fines, and water volume per cm³ of mortar.

Sample	Volume of fines (cm^3/cm^3)	Δ_{vf}	Water volume (cm^3/cm^3)	Δ_{va}	Area of fines (m^2/cm^3)	Δ_{af}
REF	0.160	–	0.257	–	0.878	–
SF40	0.199	24.38%	0.245	−4.64%	2.555	191.12%
BS40	0.198	23.71%	0.246	−4.51%	2.825	221.91%
BC40	0.207	29.30%	0.243	−5.57%	1.062	20.99%
AR40	0.217	35.93%	0.240	−6.83%	1.150	30.98%

Δ_{vf} = variation in the volume of fines; Δ_{va} = variation in water volume; Δ_{af} = variation in the area of fines.

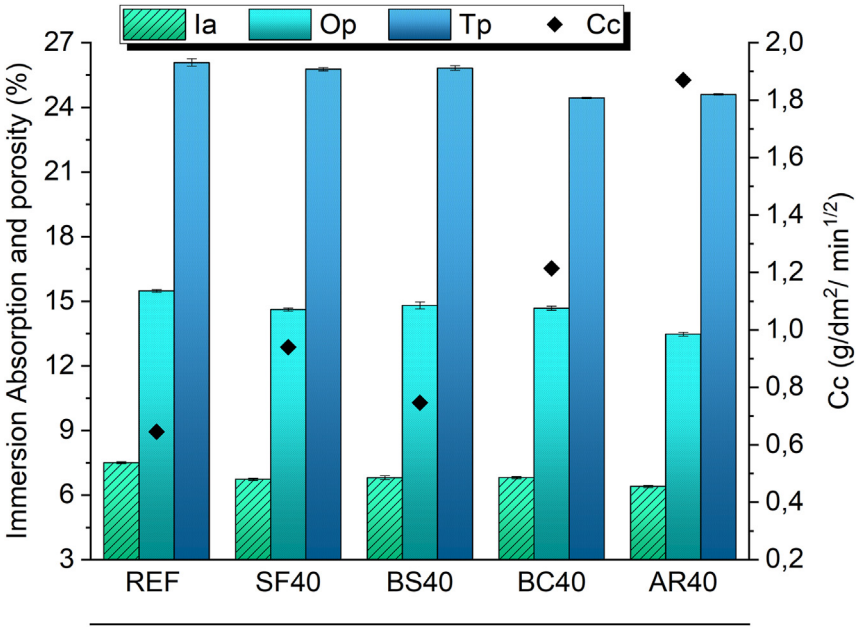

Fig. 5 – Immersion Absorption (Ia), open porosity (Op), total porosity (Tp) and capillarity coefficient (Cc) of cementitious composite.

However, a small porosity reduction due to IOT introduction was also shown, in relation to the reference sample. Nevertheless, it is worth pointing out that the method used by the software is quite sensitive to image contrast in pore definition. Variation in results was expected, although the section and region definition are typical to the material, image analysis corresponded to only a small region of the sample.

3.6. *Compressive strength*

Compressive strength results are presented in Fig. 8. In general, IOT addition to cementitious composite increased compressive strength, and this behavior was in opposition to that observed for consistency. BS40 sample presented the lowest consistency index, however, this sample exhibited the greater compressive strength (48.3 MPa), 22.9% higher than the REF sample. The BC40 and SF40 samples also presented strength improvement by 17.8% and 11.8%, respectively. Only the AR40 sample reach lower mechanical strength (2.1% loss), which can be considered irrelevant. Moreover, during the compressive strength test, a more visible brittle fracture in IOT-added cementitious composite was observed. It suggests an increase of stiffness in these materials. These results are according to Castro's [41] studies, with the same gain in strength (14%) based on the same addition content.

The influence of non-reactivity IOT on mechanical resistance is related to physical effects, such as particle packing, interaction between the cement matrix and the aggregate (adherence), nucleation effect, as well as to the effective w/c ratio. In addition, the use of IOT added to the mortars decreased the fluidity, since these materials were added to the mix while the w/c ratio remained unchanged. Therefore, part of the water is attached on the IOT and aggregate surfaces. According to area of fines presented in Table 5, it is possible to observe that samples SF40 and BS40 had their effective water/solid ratio strongly reduced, which leads a smaller effective w/c. These were the factors that may have influenced compressive strength gains.

Moreover, the influence on mechanical resistance is related to physical effects, such as filling voids and packing particle improvement, interaction between the cement matrix and the aggregate (adherence) and nucleation effect. Therefore, particle size distribution and particle surface characteristics in cementitious composite AR40 may have contributed to the difference observed in compressive strength, in comparison to that of other IOT-added cementitious composite.

3.7. *Composites microstructure*

The cement matrixes of composites are illustrated in Figs. 9 and 10, highlighting a 40 μm region from the aggregate. REF sample (Fig. 9) presented a more porous cement matrix close to the aggregates (ITZ – Interfacial Transition Zone) and there are some cracks, small unhydrated cement particles (UC) and portlandite (CH). On the other hand, it is possible to observe in IOT-added samples (Fig. 10), a void filling by IOT particles in the ITZ region. In addition, the finer the tailing particle, the closer it was to the aggregate. The accumulation of these particles can be justified by high specific mass of the IOTs, which are taken by the water and deposited in ITZ, and the addition in the volume of solids in the mix. The SF40 and BS40 samples presented larger IOT particles in the ITZ, as well as cracks in the cement matrix. It is worth noting that those tailings recorded the highest specific mass. Besides, it is possible to observe that AR40 presented matrix denser than that of the other samples, as well as smaller number of pores and cracks, similar to evidence in the porosity test. Overall, IOT-added samples did not show expressive CH formation in ITZ or around the tailing particles. This pointed out that samples can have good mechanical-property of the ITZ.

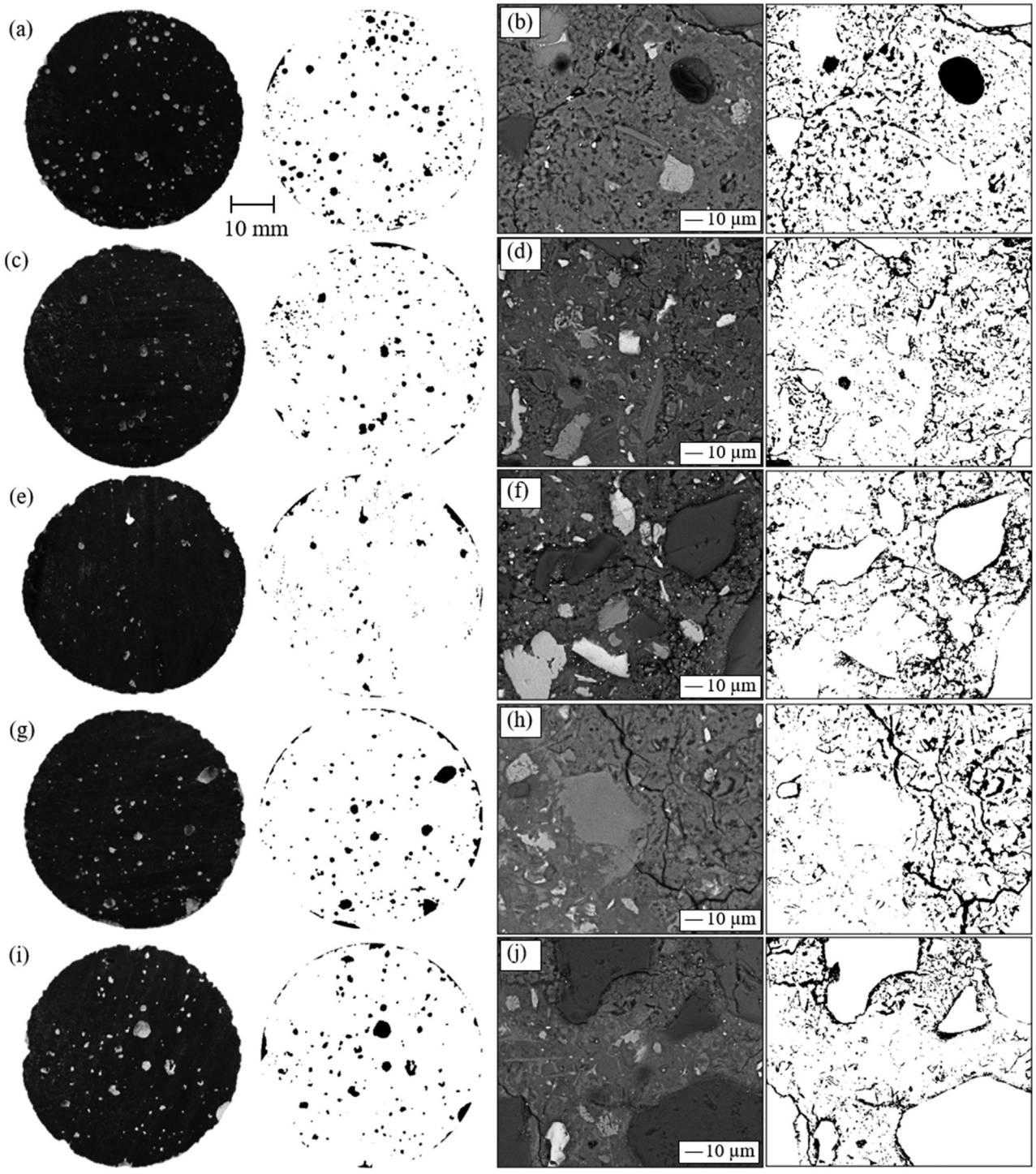

Fig. 6 – Cross-section of the specimen cementitious composite and the polished sample, highlighting the pores and fissures (a and b) REF, (c and d) SF40, (e and f) BS40, (g and h) BC40, (i and j) AR40.

According to Zhao et al. [35], some IOT particles presenting a porous surface can absorb water during the mixing, and it promotes the adequate environment for CH growth during hydration. This effect was not observed in samples with porous IOT (SF40 and BS40), likely due to the lower particle size of IOTs in this study, in comparison to that of research that have used IOT with aggregate.

Han et al. [59] highlighted that there may be low adhesion of the surrounding hydrated compounds in samples presenting low porosity and roughness, and the poor ligation to the matrix can be a point of low resistance to loads. However, in the present study, tailing particles seemed to have good adherence to the cement paste. This may be related to the particle size distribution of the tailings, which is smaller in

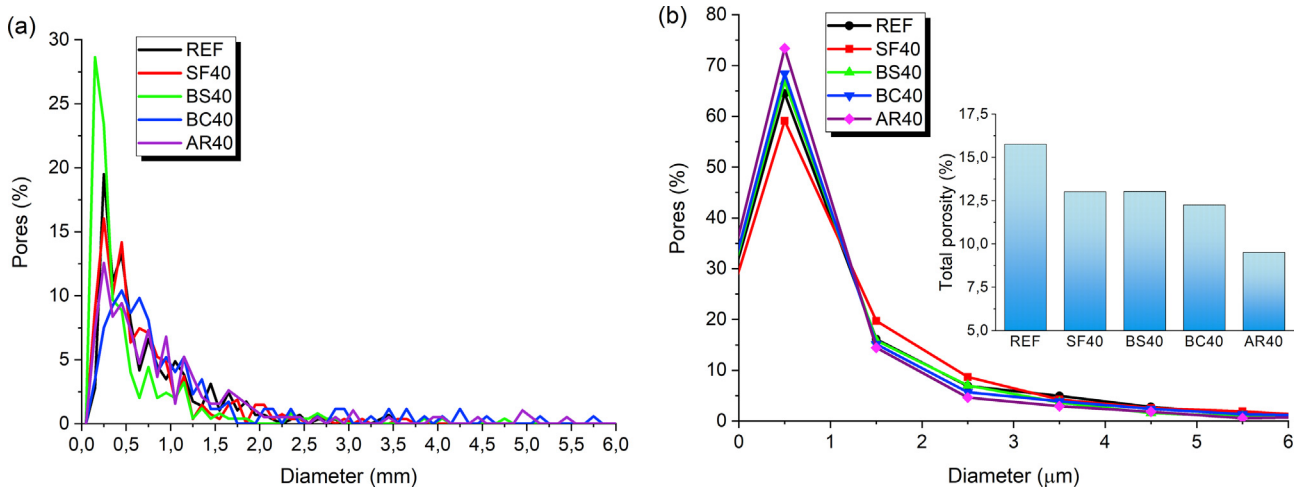

Fig. 7 – Pore diameter distribution of the specimens' cross-section: (a) digital microscope image and (b) SEM image.

this study, compared to these author's study. Tailing particles have properly adhered to the cement paste, even in samples more porous (SF40) and with IOT which has smoother surface and lowest SSA (AR40). Therefore, IOT adherence to the matrix seemed not to be significantly affected by the physical properties of the material, since samples SF and AR had different properties.

3.8. *Dynamic elastic modulus and density*

Dynamic elastic modulus and density of composites are shown in Fig. 11. According to results, it was observed that the greater the specific mass of the IOT, the greater the specific mass of the cementitious composite and, consequently, the greater its modulus of elasticity. Cementitious composite SF40 and BS40, which recorded the highest specific dry mass, showed increase in the modulus of elasticity by 11.67% and 17.97%, respectively, in comparison to the reference. BC40 and AR40 samples presented gains by 10.55% and 8.22%, respectively. It is important to highlight that the high specific mass of the IOTs contributed to increase the apparent density of the cementitious composite. Consequently, the higher the density, the faster the wave propagation speed and the higher the rigidity [47]. Accordingly, the lower specific mass of the AR tailing justified the lower density and modulus of elasticity of cementitious composite AR40 in comparison to other IOT-added composites.

IOT addition led to formation of a denser matrix and a good-dispersion of fine pores, which has contributed to gains in rigidity. This was also observed by Carrasco et al. [8], by replacing the sand for IOT. Further, IOT mechanical properties are also important factors, since modulus of elasticity of the composite depend on the modulus of the materials that compose it. According to Zhao et al. [27], IOT's indentation module stays close to the natural aggregates.

3.9. *Electrical resistivity*

There is a consensus in the literature that electrical resistivity and the corrosive environment have a reversed relationship in reinforced concrete [59,66]. Whiting and Nagi [60] presented

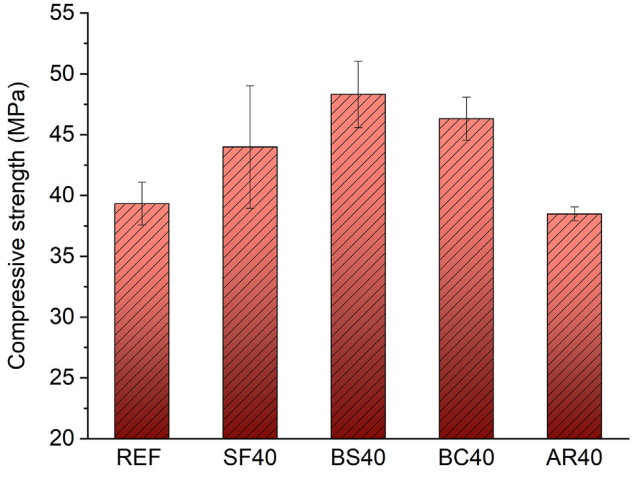

Fig. 8 – Compressive strength of cementitious composite (28 days).

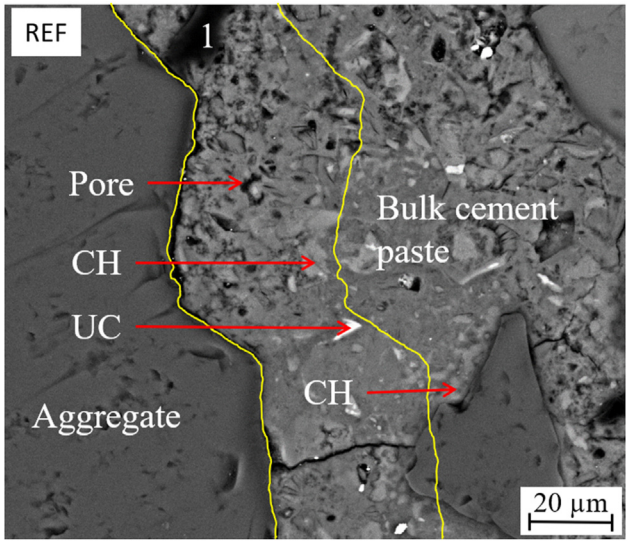

Fig. 9 – SEM-BSE image of REF sample.

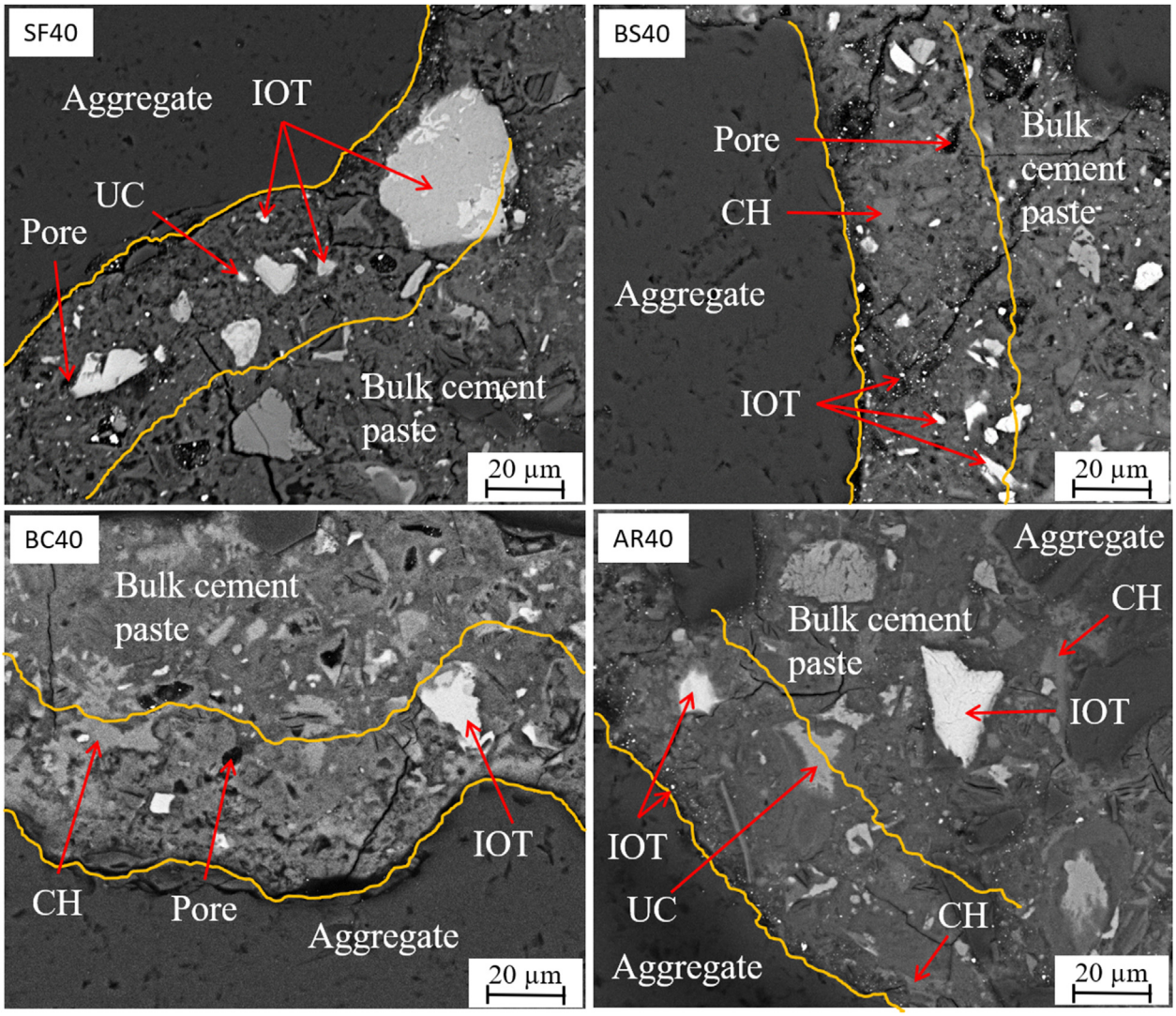

Fig. 10 – SEM-BSE images of IOT-added samples.

the potential corrosion limits for concrete depending on electrical resistivity, which is: "too high" (<50 Ω.m); "high" (50–100 Ω.m); "moderate to low" (100–200 Ω.m) and "low" (>200 Ω.m). Based on the electrical resistivity results of composites, shown in Fig. 12, all composites would fit the "too high" concrete armor's corrosion potential band. Nevertheless, as reported by Hou et al. [29], this property is quite influenced by big aggregates, which can present very high resistivity. These authors have found resistivity of 33 Ω.m in mortar presenting composition ratio of 1:1 and w/c of 0.40. These values are close to those recorded in the present study. Hence, because electrical resistivity values regard a structural mortar, without big aggregates, they were expected to present lower values.

Usually, the cementitious matrix was the route presenting the lowest electrical resistivity due to the porous structure of the C–S–H gel and to the pore solution inside it [29]. According to Medeiros Júnior and Lima [61] and Ramezanianpour et al. [62], cementitious supplementary materials, such as fly ash, silica fume and blast furnace slag, can reduce the size of cement paste pores, limit electric conduction through the pore solution and produce concrete with higher strength. Thus, matrix densification would increase electrical resistivity. However, despite the low

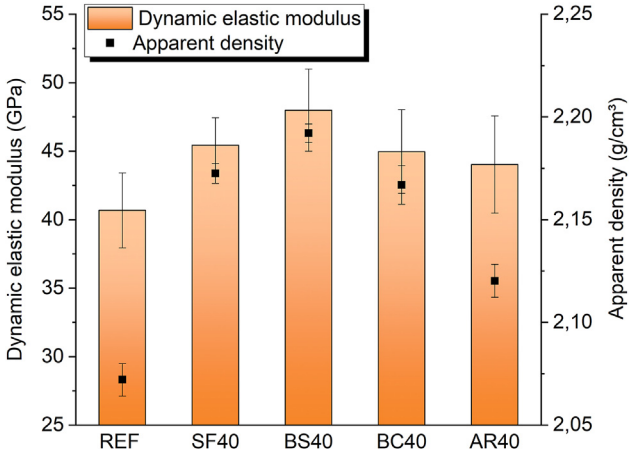

Fig. 11 – Dynamic elastic modulus and apparent density of cementitious composite.

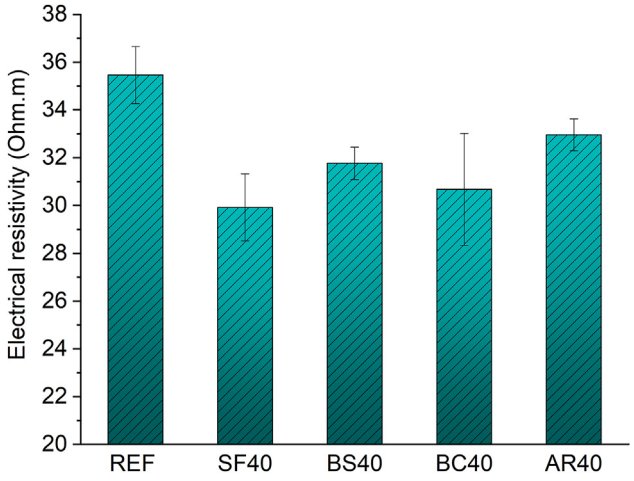

Fig. 12 – Electrical resistivity of cementitious composite.

reduction in the porosity of the cementitious composite caused by IOT addition, composites presented decreased electrical resistivity.

Yet, the reduction observed in the w/c ratio increased pore solution conductivity due to increased ionic concentration inside it [59]. Thus, effective w/c ratio reduction in IOT-added composite, due to increased volume of solids, may have been one of the accountable reasons for the reduced resistivity in these samples. Furthermore, it is important pointing out that the presence of iron oxides in IOTs, such as hematite and magnetite, can increase the cementitious composites' conductivity, due to the electric properties of this mineral, as shown in the study by Martini et al. [63].

Variation in this property among IOT-added samples was not very significant (10%, at most, between SF40 and AR40), and IOT heterogeneity had low influence on it. It is important highlighting that this value was slightly higher than that recorded for sample AR40, assumingly due to the lower open porosity of the sample and to the presence of more refined capillarity.

3.10. *Accelerated carbonation*

Fig. 13a presents carbonation depth in cementitious composite and Fig. 13b illustrates the specimens after carbonation and phenolphthalein solution aspersion. According to the results, it was possible to observe that IOT addition has reduced carbonation in the cementitious composite. The REF sample reach carbonation of 8.51 mm, whereas IOT-added cementitious composite showed a decrease in this value. The AR40 sample showed 0 mm (median value) in carbonation depth. Such a reduction can be justified by lower porosity and pore refinement in IOT-added composites, mainly in AR40. There was no significant variation in results among the other IOT-added samples (SF40, BS40 and BC40), and this finding is indicative that heterogeneity tends not to be a great-impact factor in this property.

According to the possibility of having corrosion in the concrete armors, the IOT-added cementitious composite has presented good behavior and indicated better durability than the reference cementitious composite. Overall, all samples recorded carbonation depth values lower than the minimum coverage (20 mm) set by the NBR 6118 Standard [64], for reinforced concrete elements, at aggressiveness class I. Similar results were observed by Shettima et al. [25] and Tian et al. [26]. Both researchers used IOT to replace small aggregates and densified the structure of the composite. However, Tian et al. [26] highlighted that carbonation speed in the oldest IOT-added composites was faster.

3.11. *Pore solution pH development*

Based on the study by Cascudo [65], the carbonation advancement behavior of concretes with different mineral additions vary. Accordingly, carbonation depth and speed depend on several factors intrinsic to concrete, rather than just to pores. This refers to CO_2 diffusion dynamics, but also on the alkaline reserve in the liquid phase, based on the chemical composition of the materials [65]. Thus, in order to complete the analysis applied to the accelerated carbonation,

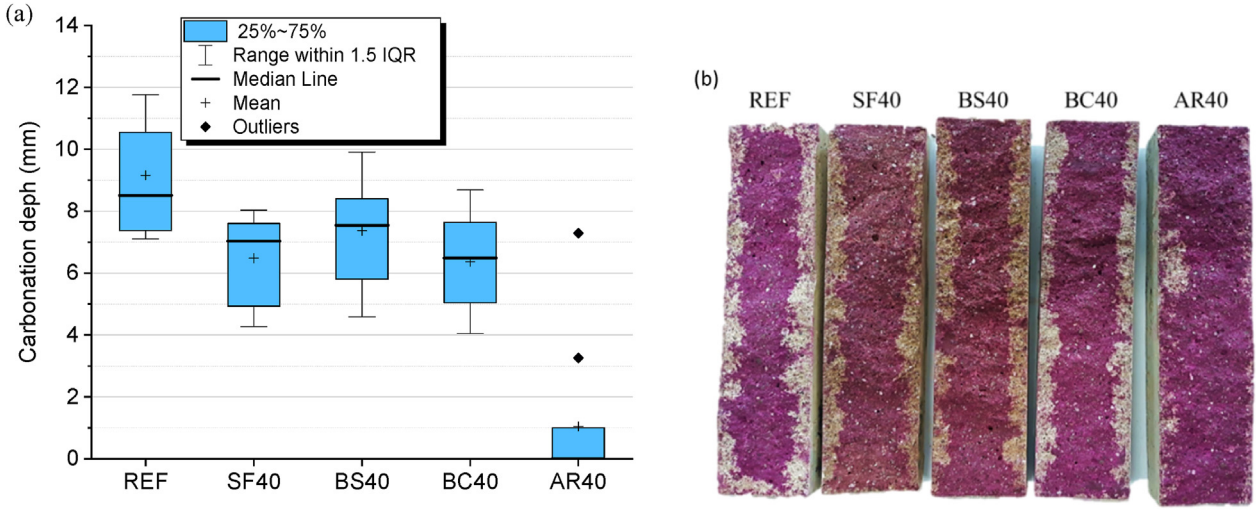

Fig. 13 – (a) Carbonation depth of cementitious composite and (b) specimens after phenolphthalein solution aspersion.

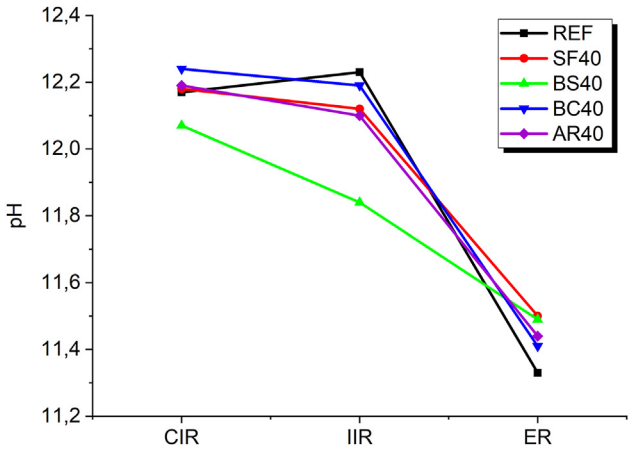

Fig. 14 – pH development of the cementitious composite pore solution after carbonation - CIR: central inner region; IIR: intermediate internal region; ER: external region.

Fig. 14 presents the study on pH development at different depths in the specimens after carbonation.

Overall, there was a pH reduction trend from the most internal region to the most external one. Based on the results, pH tended to be higher than that in the reference cementitious composite in the external region of IOT-added cementitious composite. This finding is in compliance with results recorded for the assay with phenolphthalein solution. Thus, porosity reduction and, consequently, CO_2 diffusion reduction, decreased carbonation in the samples and was an important aspect to the herein recorded results.

It is important to highlight that the IIR region, which is located approximately 1 cm from the edge, was within the alkaline band in all cementitious composites, similar to results of the phenolphthalein method. Thus, values lower than 8.4–9.8 were expected to happen (phenolphthalein turning range) [51]. However, it was not observed since the pore solution of all cementitious composite resulted in pH close to 11.4. According to McPolin et al. [51], this number can be explained by the greater concentration of OH^- deriving from non-moistened cement particles that were taken to suspension when the mortar was turned into powder. Based on such a method, pH differences among samples were not seen as representative.

4. Conclusion

Four IOT samples studied had different physical properties and chemical/mineralogical compositions. The characterization results suggests that the higher the degree of ore processing, the smaller the heterogeneity, the iron content and specific masses.

IOT addition in composites reduced the consistency index and this effect was stronger when SSA and IOT porosity were higher. IOT addition also led to maintenance, with a trend to reduce, porosity and absorption of the cementitious composite. Nevertheless, there was great variation in capillarity coefficient. This finding was confirmed by SEM images, which have shown that the cementitious matrices in the IOT-added samples were denser and presented localized higher-porosity regions. Overall, the physical properties of the IOTs have influenced (increased) the capillarity of cementitious composite.

In composites' mechanical properties, the IOT addition increased compressive strength, which presented reversed behavior to that observed for consistency. It may be explained due to effective w/c ratio reduction, cement matrix densification (filler effect) and a good adherence of aggregate-cement matrix, mainly in IOTs samples with higher SSA. The pore filling effect also led to an increase in modulus of elasticity, being higher for samples with higher specific mass and composites with lower porosity.

Electrical resistivity of IOT-added cementitious composite remained at the same order of magnitude of the reference and at the same corrosion potential. However, there was reduction trend due to IOT addition, despite the porosity reduction, due to the presence of conductive minerals, such as hematite and magnetite. The carbonation depth recorded for IOT-added cementitious composite was lower than that of the reference. Therefore, the use at 40% addition content allowed producing good structural resistance and durability in cementitious composite. However, the influence of IOT heterogeneity on cementitious composite was identified. Thus, this factor must be considered at the application of different materials.

Declaration of Competing Interest

The authors declare that they have no known competing financial interests or personal relationships that could have appeared to influence the work reported in this paper.

Acknowledgement

The research team is grateful to the mining companies for providing the iron ore tailings and to the funding agencies National Counsel for Technological and Scientific Development (CNPq), Coordination for the Improvement of Higher Education Personnel (CAPES) and Research Support Foundation of Minas Gerais (FAPEMIG) for the support provided to this study.

REFERENCES

[1] United State Geological Survey (USGS). National minerals information center – mineral commodity summaries. 2019. https://www.usgs.gov/centers/nmic/iron-ore-statistics-and-information. [Accessed 9 September 2019].
[2] Brazilian Mining Institute (IBRAM), Mineral economy of Brazil. https://agenciabrasil.ebc.com.br/geral/noticia/2020-02/ibram-producao-de-minerio-em-2019-caiu-mas-faturamento-cresceu. [Accessed 29 August 2021].
[3] G1. Tailings from dams reach areas up to 100 km in MG. 2015. http://g1.globo.com/minas-gerais/noticia/2015/11/hidreletrica-100-km-e-afetada-por-lama-do-rompimento-de-barragens.html. [Accessed 6 November 2019].
[4] G1. Brumadinho: sobe para 249 o número de mortos no rompimento da barrage. 2019. https://g1.globo.com/mg/minas-gerais/noticia/2019/08/31/brumadinho-sobe-para-

249-o-numero-de-mortos-no-rompimento-de-barragem.ghtml. [Accessed 18 December 2019].
[5] Almada BS, Cancio AS, Duarte MS, Farjardo AA, Santos WJ. Use of iron ore tailings as a mineral addition to cement composites. In: Strength, growth and quality of civil engineering in Brazil. 3rd ed. 2021. p. 25–38. https://doi.org/10.22533/at.ed.8062112043 [Chapter 3].
[6] Dauce PD, Castro GB, Lima MMF, Lima RMF. Characterisation and magnetic concentration of an iron ore tailings. J Mater Res Technol 2018;8(1):1052–9. https://doi.org/10.1016/j.jmrt.2018.07.015.
[7] Institute for Technological Research (IPT). Waste treatment is an economically viable alternative solution to the mining dam. 2016. http://www.ipt.br/noticias_interna.php?id_noticia=1043. [Accessed 16 August 2019].
[8] Carrasco EVM, Magalhães MDC, Santos WJ, Alves RC, Mantilla JN. Characterization of mortars with iron ore tailings using destructive and nondestructive tests. Construct Build Mater 2017;131:31–8. https://doi.org/10.1016/j.conbuildmat.2016.11.065.
[9] Fontes WC, Mendes JC, Silva SN, Peixoto RAF. Mortars for laying and coating produced with iron ore tailings from tailing dams. Construct Build Mater 2016;112:988–95. https://doi.org/10.1016/j.conbuildmat.2016.03.027.
[10] Souza AT, Barbosa TF, Riccio LA, Santos WJ. Effect of limestone powder substitution on mechanical properties and durability of slender precast components of structural mortar. J Mater Res Technol 2019;9:847–56. https://doi.org/10.1016/j.jmrt.2019.11.024.
[11] Viana TM, Bacelar BA, Coelho ID, Ludvig P, Santos WJ. Behaviour of ultra-high performance concretes incorporating carbon nanotubes under thermal load. Construct Build Mater 2020;263:1–8. https://doi.org/10.1016/j.conbuildmat.2020.120556.
[12] Yellishetty M, Karpeb V, Reddyb EH, Subhashb KN, Ranjitha PG. Reuse of iron ore mineral wastes in civil engineering constructions: a case study. Resour Conserv Recycl 2008;52:1283–9. https://doi.org/10.1016/j.resconrec.2008.07.007.
[13] Peixoto RF, Mendes JC, Fontes WC, Bastos LAC, Sant'anna JN, Santos DH. Use of iron ore dam tailings in civil construction. Reciclos Technical Report. UFOP; 2016. p. 56.
[14] Silva FL, Araújo FGS, Teixeira MP, Gomes RC, Von Kruger FL. Study of the recovery and recycling of tailings from the concentration of iron ore for the production of ceramic. Ceram Int 2014;40:16085–9. https://doi.org/10.1016/j.ceramint.2014.07.145.
[15] Weishi L, Guoyuan L, Ya X, Qifei H. The properties and formation mechanisms of eco-friendly brick building materials fabricated from low-silicon iron ore tailings. J Clean Prod 2018;204:685–92. https://doi.org/10.1016/j.jclepro.2018.08.309.
[16] Bastos LAC. Using iron ore tailings from tailing dams as road. Mater J Mater Civ Eng 2016;28:988–95. https://doi.org/10.1061/(ASCE)MT.1943-5533.0001613.
[17] Borges PHR, Ramos FCR, Caetano TR, Panzerra TH, Hersilia S. Reuse of iron ore tailings in the production of geopolymer mortars, Revista Escola de Minas. Int Eng J Ouro Preto 2019;72(4):581–7. https://doi.org/10.1590/0370-44672017720169.
[18] Galvão JLB, Andrade HD, Brigolini GJ, Peixoto RAF, Mendes JC. Reuse of iron ore tailings from tailings dams as pigment for sustainable paints. J Clean Prod 2018;200:412–22. https://doi.org/10.1590/0370-44672017720169.
[19] Feng XX, Xi XL, Cai JW, Chai HJ, Song YZ. Investigation of drying shrinkage of concrete prepared with iron mine tailings. Key Eng Mater 2011;477:37–41. https://doi.org/10.4028/www.scientific.net/KEM.477.37.
[20] Liu W, Xu X, An Y. Study on the sprayed concrete with iron tailings. Adv Mater Res 2012;347–353:1939–43. https://doi.org/10.4028/www.scientific.net/AMR.347-353.1939.
[21] Yu L, Zhang J, Mu K. Relationships between compressive strength and microstructure in mortars with iron ore tailings as fine aggregate. Appl Mech Mater 2012;188:211–8. https://doi.org/10.4028/www.scientific.net/AMM.188.211.
[22] Guodong Z, Xiuzhi Z, Zonghui Z, Xin C. Preparation and properties of concrete containing iron tailings/manufactured sand as fine aggregate. Adv Mater Res 2014;838–841:152–5. https://doi.org/10.4028/www.scientific.net/AMR.838-841.152.
[23] Kuranchie FA, Shukla SK, Habibi D, Mohyeddin A. Utilization of iron ore tailings as aggregates in concrete. Cogent Engineering 2015;2(1). https://doi.org/10.1080/23311916.2015.1083137.
[24] Goyal S, Singh K, Hussain A, Singh PR. Study on partial replacement of sand with iron ore tailing on compressive strength of concrete. Int J Res Eng Adv Technol 2015;3(2):243–8.
[25] Shettima AU, Hussin MW, Ahmad Y, Mirza J. Evaluation of iron ore tailings as replacement for fine aggregate in concrete. Construct Build Mater 2016;120:72–9. https://doi.org/10.1016/j.conbuildmat.2016.05.095.
[26] Tian Z, Zhao Z, Dai C, Liu S. Experimental study on the properties of concrete mixed with iron ore tailings. Adv Mater Sci Eng 2016:8606505. https://doi.org/10.1155/2016/8606505.
[27] Gu X, Zhang W, Zhang X, Li X, Qiu J. Hydration characteristics investigation of iron tailings blended ultra-high-performance concrete: the effects of mechanical activation and iron tailings content. J Build Eng 2022;45:103459. https://doi.org/10.1016/j.jobe.2021.103459.
[28] Filho JS, Silva SN, Silva GC, Mendes JC, Peixoto RAF. Technical and environmental feasibility of interlocking concrete pavers with iron ore tailings from tailings dams. Construct Build Mater 2017;29:1–7. https://doi.org/10.1061/(ASCE)MT.1943-5533.0001937.
[29] Hou T, Nguyen VK, Su Y, Chen Y, Chen P. Effects of coarse aggregates on the electrical resistivity of Portland cement concrete. Construct Build Mater 2017;133:397–408. https://doi.org/10.1016/j.conbuildmat.2016.12.044.
[30] Shettima AU, Ahmad Y, Hussin MW, Muhammad NZ, Babatude OE. Strength and microstructure of concrete with iron ore tailings as replacement for river sand. In: E3S Web of Conferences, International Conference on Civil and Environmental Engineering, vol. 34; 2018. https://doi.org/10.1051/e3sconf/20183401003.
[31] Yi Z, Sun H, Wei X, Li C. Iron ore tailings used for the preparation of cementitious material by compound thermal activation. Int J Miner Metall Mater 2009;16:355–8. https://doi.org/10.1016/S1674-4799(09)60064-9.
[32] Luo L, Zhang Y, Bao S, Chen T. Utilization of iron ore tailings as raw material for Portland cement clinker production. Adv Mater Sci Eng 2016:1596047. https://doi.org/10.1155/2016/1596047.
[33] Yunhong C, Fei H, Wenchuan L, Riu L, Guanglu L, Jingming W. Test research on the effects of mechanochemically activated iron tailings on the compressive strength of concrete. Construct Build Mater 2016;118:164–70. https://doi.org/10.1016/j.conbuildmat.2016.05.020.
[34] Han F, Li L, Song S, Liu J. Early-age hydration characteristics of composite binder containing iron tailing powder. Powder Technol 2017;3015:322–31. https://doi.org/10.1016/j.powtec.2017.04.022.

[35] Xiong C, Li W, Jiang L, Wang W, Guo Q. Use of grounded iron ore tailings (GIOTs) and $BaCO_3$ to improve sulfate resistance of pastes. Construct Build Mater 2017;150:66–76. https://doi.org/10.1016/j.conbuildmat.2017.05.209.
[36] Magalhães LF, Morais IS, Esteves Junior MA, Melo AC, Maia ALF, Bezerra ACS. Resistance to acid attack of Portland cement with added iron ore tailings. In: 59th Brazilian concrete Congress; 2017.
[37] Young G, Yang M. Preparation and characterization of portland cement clinker from iron ore tailings. Construct Build Mater 2019;197:152–6. https://doi.org/10.1016/j.conbuildmat.2018.11.236.
[38] Yao G, Wang Q, Su Y, Wang J, Qiu J, Lyu X. Mechanical activation as an innovative approach for the preparation of pozzolan from iron ore tailings. Miner Eng 2020;145:106068. https://doi.org/10.1016/j.mineng.2019.106068.
[39] Cheng Y, Huang F, Qi S, Li W, Liu R, Li G. Durability of concrete incorporated with siliceous iron tailings. Construct Build Mater 2020;242:118147. https://doi.org/10.1016/j.conbuildmat.2020.118147.
[40] Magalhães LF, Morais IS, Lara LFS, Resende DS, Menezes RMRO, Aguilar MTP, et al. Iron ore tailing as addition to partial replacement of Portland cement. Mater Sci Forum 2018;930:125–30. https://doi.org/10.4028/www.scientific.net/MSF.930.125.
[41] Castro NLB, Almada BS, Fajardo AA, Oliveira CA, Santos WJ. Influence of addition contents of iron ore tailings on structural mortar. J Manag Sustain 2021;11(1). https://doi.org/10.5539/jms.v11n1p74.
[42] Huang X, Ranade R, Li VC. Feasibility study of developing green ECC using iron ore tailings powder as cement replacement. J Mater Civ Eng 2013;25(7):923–31. https://doi.org/10.1061/(ASCE)MT.1943-5533.0000674.
[43] ASTM - American Society for Testing and Materials. C39 - standard test method for compressive strength of cylindrical concrete specimens. 2015. https://doi.org/10.1520/C0039.
[44] British Adopted European Standard. BS EN 1015-3: methods of test for mortar for masonry Part 3: determination of consistence of fresh mortar (by flow table). 1999. Brussels.
[45] British Adopted European Standard. BS EN 1015-11: methods of test for mortar for masonry. Determination of flexural and compressive strength of hardened mortar. 1999. Brussels.
[46] American Society for Testing and Materials. ASTM C215-19: standard test method for fundamental transverse, longitudinal, and torsional resonant frequencies of concrete specimens. West Conshohocken, PA: ASTM International; 2019.
[47] Lee BJ, Kee S-H, Oh T, Kim Y-Y. Effect of cylinder size on the modulus of elasticity and compressive strength of concrete from static and dynamic tests. Adv Mater Sci Eng 2015:1–12. https://doi.org/10.1155/2015/580638.
[48] ABNT - Brazilian Association of Technical Norms. NBR 9204: hardened concrete—determination of the electrical-volumetrical resistivity—test method. 2012.
[49] RILEM - Réunion Internationale des Laboratoires D'essais et de Recherches Sur Les Matériaux Et Les Constructions. CPC 18: measurement of hardened concrete carbonation depth. Mater Struct 1988;21:453–5.
[50] International Organization for Standardization. ISO 1920-12: testing of concrete - Part 12: determination of the carbonation resistance of concrete—accelerated carbonation method. 2015.
[51] McPolin DO, Basheer PAM, Long AE. Carbonation and pH in mortars manufactured with supplementary cementitious materials. J Mater Civ Eng 2009;21(5):217–25. https://doi.org/10.1061/_ASCE_0899-1561(2009)21:5(217).
[52] American Society for Testing and Materials. ASTM C642-13: standard test method for density, absorption, and voids in hardened concrete. 2013. Pennsylvania.
[53] British Adopted European Standard. BS EN 1015-18: methods of test for mortar for masonry. Determination of water absorption coefficient due to capillary action of hardened mortar. 2002. Brussels.
[54] Scrivener KL. Backscattered electron imaging of cementitious microstructures: understanding and quantification. Cem Concr Compos 2004;26:935–45. https://doi.org/10.1016/j.cemconcomp.2004.02.029.
[55] Kjellsen KO, Detwiler RJ, Gjørv OE. Backscattered electron image analysis of cement paste specimens: specimen preparation and analytical methods. Cement Concr Res 1991;21(2–3):388–90. https://doi.org/10.1016/0008-8846(91)90020-I.
[56] Diamond S. Considerations in image analysis as applied to investigations of the ITZ in concrete. Cem Concr Compos 2001;23:171–8. https://doi.org/10.1016/S0958-9465(00)00085-8.
[57] Tang C, Li K, Ni W, Fan D. Recovering iron from iron ore tailings and preparing concrete composite admixtures. Minerals 2019;9(232). https://doi.org/10.3390/min9040232.
[58] Mehta PK, Monteiro PJM. Concrete: properties and materials, 2a. São Paulo: IBRACON; 2014.
[59] Azarsa P, Gupta R. Electrical resistivity of concrete for durability evaluation: a review. Adv Mater Sci Eng 2017:30. https://doi.org/10.1155/2017/8453095.
[60] Whiting DA, Nagi MA. Electrical resistivity of concrete-a literature review. Portland Cemente Association R&D; 2003. p. 2457 2457.
[61] Medeiros-Junior RA, Lima MG. Electrical resistivity of unsaturated concrete using different types of cement. Construct Build Mater 2016;107:11–6. https://doi.org/10.1016/j.conbuildmat.2015.12.168.
[62] Ramezanianpour AA, Pilvar A, Mahdikhani M, Moodi F. Practical evaluation of relationship between concrete resistivity, water penetration, rapid chloride penetration and compressive strength. Construct Build Mater 2011;25(5):2472–9. https://doi.org/10.1016/j.conbuildmat.2010.11.069.
[63] Martini RJ, Caetano TR, Santos HA, Aranha PRA. Deposition of iron ore tailings in reservoirs: an application of the GPR method. Ambiente Água Interdiscip J Appl Sci 2016;11(4). https://doi.org/10.4136/ambi-agua.1831.
[64] ABNT - Brazilian Association of Technical Norms. NBR 6118: design of concrete structures – Procedure. 2014.
[65] Cascudo O, Pires P, Carasek H, Castro A, Lopes A. Evaluation of the pore solution of concretes with mineral additions subjected to 14 years of natural carbonation. Cement Concr Compos 2021;115. https://doi.org/10.1016/j.cemconcomp.2020.103858.
[66] Sang Y, Yang Y, Zhao Q. Electrical resistivity of plain cement-based materials based on ionic conductivity: a review of applications and conductive models. J Build Eng 2021:103642. https://doi.org/10.1016/j.jobe.2021.103642.